Journal of Biomechanics 88 (2019) 122–129

Contents lists available at ScienceDirect

Journal of Biomechanics

journal homepage: www.elsevier.com/locate/jbiomech
www.JBiomech.com

A critical comparison of different residence time measures in aneurysms

Mirza Md Symon Reza, Amirhossein Arzani *

Mechanical Engineering Department, Northern Arizona University, Flagstaff, AZ, USA

ARTICLE INFO

Article history:
Accepted 20 March 2019

Keywords:
Flow stagnation
Hemodynamics
Blood flow
Thrombosis
Transport

ABSTRACT

Flow stagnation and residence time (RT) are important features of diseased arterial flows that influence biochemical transport processes and thrombosis. RT calculation methods are classified into Eulerian and Lagrangian approaches where several measures have been proposed to quantify RT. Each of these methods has a different definition of RT, and it is not clear how they are related. In this study, image-based computational models of blood flow in an abdominal aortic aneurysm and a cerebral aneurysm were considered and RT was calculated using different methods. In the Lagrangian methods, discrete particle tracking of massless tracers was used to calculate particle residence time and mean exposure time. In the Eulerian methods, continuum transport models were used to quantify RT using Eulerian RT and virtual ink approaches. Point-wise RT and Eulerian indicator RT were also computed based on measures derived from velocity. A comparison of these methods is presented and the implications of each method are discussed. Our results highlight that most RT methods have a conceptually distinct definition of RT and therefore should be utilized depending on the specific application of interest.

1. Introduction

Aneurysms are abnormal vessel enlargements with high morbidity and mortality rates in the aging population. Abdominal aortic aneurysm (AAA) and cerebral aneurysm (CA) are the two most common and fatal kind of aneurysms (Humphrey and Taylor, 2008). Rupture of AAA records an overall mortality rate of 90% (Assar and Zarins, 2009) and rupture of CA carries about 45% mortality rate (Brisman et al., 2006). Blood flow and hemodynamics are believed to influence the pathogenesis and pathophysiology of aneurysms. One pathway connected with blood flow is transport of biochemicals and cells in blood. Particularly, flow stagnation and high residence time (RT) of specific biochemicals play a crucial role in known complications associated with aneurysms such as thrombosis and vessel wall inflammation. Flow stagnation is part of Virchow's triad for thrombus formation (Lowe, 2003; Dickson, 2004), and near-wall stagnation and build-up of inflammatory cells such as monocytes contribute to vessel wall inflammation (Raffort et al., 2017).

Image-based computational fluid dynamics (CFD) modeling has become a popular method to obtain blood flow data and subsequently quantify various hemodynamic measures. Such methods have been used to spot connections between hemodynamics and aneurysm growth and rupture (Boussel et al., 2008; Meng et al., 2013; Martufi and Gasser, 2013). Previous studies have underlined that regions of high flow recirculation and stagnation may allow building a higher concentration of platelets and platelet-derived factors (Suh et al., 2011b; Kunov et al., 1996; Perktold, 1987). These changes may prompt thrombosis initiation on the aneurysm wall, which may increase the risk of aneurysm expansion and rupture (Satta et al., 1996; Wolf et al., 1994). Rayz et al. (2010) have found a correlation between regions where thrombus deposition occur in vivo and where CFD predicted elevated RT and low wall shear stress (WSS). It has been shown that stagnation is required for effective atherogenic processes (Chiu et al., 2003). It is hypothesized that low WSS and high RT act as hemodynamic risk factors for vascular disease (Ku et al., 1985; Nerem, 1992).

These studies have supported the importance of flow stagnation and RT in cardiovascular disease. Numerous definitions of RT have been proposed and utilized in various studies. Lagrangian and Eulerian approaches are two classes of methods to evaluate RT. Lagrangian methods are based on tracking particles (typically massless tracers) advected by the flow and calculating a measure representing RT, while Eulerian methods define RT by either solving a partial differential equation or proposing a measure based on velocity vectors. The most common Lagrangian approach is particle residence time (PRT), in which particles are released in the flow and their spatial positions are traced over time to identify the time each particle resides in the domain (Suh et al., 2011b,a; Butty et al., 2002; Duvernois et al., 2013; Arzani et al., 2014a). The second Lagrangian approach for measuring RT is mean exposure time

* Corresponding author.
E-mail address: amir.arzani@nau.edu (A. Arzani).

https://doi.org/10.1016/j.jbiomech.2019.03.028
0021-9290/

(MET) or sometimes called volumetric residence time where particles are released in the domain and the normalized cumulative time of all the particles staying inside a subdomain is measured (Lonyai et al., 2010; Sengupta et al., 2012; Duvernois et al., 2013; Arzani et al., 2014b; Kunov et al., 1996; Tambasco and Steinman, 2002). In the Eulerian approach, a continuum advection-diffusion equation with a constant source term is solved to track the accumulation of time at each location (Esmaily-Moghadam et al., 2013). This method has been used to model thrombus formation in a stenosis (Narracott et al., 2005) as well as flow stagnation in pulsatile ventricular assist devices (Long et al., 2014) and the left ventricle (Rossini et al., 2016). Another technique was developed to measure RT in an Eulerian framework where virtual-ink is infused and the time it takes to leave the region of interest is measured (Rayz et al., 2010; Epshtein and Korin, 2018). Finally, simple measures based on the velocity vector field have been proposed to estimate RT in a simple manner (McIlhany and Wiggins, 2012; Esmaily-Moghadam et al., 2013).

Each of the aforementioned definitions of RT has been used in different cardiovascular flow applications. However, we do not yet understand how these methods are related and there is a need to establish a clear consensus of these techniques. In this study, the aforementioned RT methods are implemented and compared in image-based aneurysms where flow stagnation is of clinical interest.

2. Methods

Fig. 1 shows the full AAA and CA computational models, and the highlighted region shows the region of interest where the different RT measures explained bellow are quantified and analyzed.

2.1. Computational fluid dynamics (CFD)

The CA simulation was done using the finite-element CFD solver, Oasis (Mortensen and Valen-Sendstad, 2015). An internal carotid artery aneurysm model was selected from the Aneurisk online database (Aneurisk ID: C0042). The model was meshed with SimVascular (Updegrove et al., 2017). The mesh had 6.24 M linear tetrahedral elements. A population-averaged pulsatile flow waveform (Hoi et al., 2010) was scaled to the inlet of the model (Valen-Sendstad et al., 2015). Zero traction boundary condition was prescribed at the outlets. The simulation time step divided the cardiac cycle into 10,000 time steps. Rigid wall and Newtonian blood rheology assumptions were made.

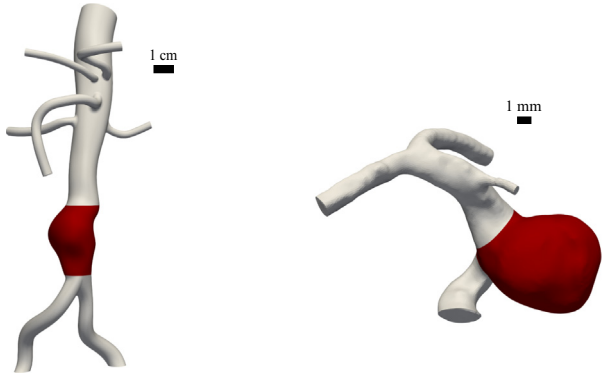

Fig. 1. The full computational models of abdominal aortic aneurysm (AAA) and cerebral aneurysm (CA) where image-based CFD was performed. The highlighted region shows the region of interest where post-processing and RT calculation was performed.

Velocity data for the AAA model were obtained from patient-specific CFD simulations performed in prior studies (Les et al., 2010; Arzani and Shadden, 2012) using SimVascular (Updegrove et al., 2017). The computational mesh had 8.53 M linear tetrahedral elements and the time step divided the cardiac cycle into 1000 time steps. Details about the CFD simulation are provided in (Les et al., 2010; Arzani and Shadden, 2012).

2.2. Lagrangian methods

2.2.1. Particle residence time (PRT)

PRT is a discrete approach of computing RT inside a flow domain from particle trajectory data. In this approach, a number of tracers (massless particles) are seeded inside the region of interest and allowed to move along with the flow. The minimum time a particle takes to leave the predefined region of interest is traced back to the initial position of the released particle, which can vary with time. This defines the PRT field, which varies in space and time (Shadden and Arzani, 2015)

$$\mathrm{PRT}(\mathbf{x}_0, t_0; \Gamma) = \min(t) \in (0, \infty) \text{ s.t. } \mathbf{x}(\mathbf{x}_0, t_0 + t) \notin \Gamma, \tag{1}$$

where $\mathbf{x}_0$ is the initial position of a particle, Γ is the region of interest, and $\mathbf{x}(t) = \mathbf{x}(t_0) + \int_{t_0}^{t} \mathbf{u}(\mathbf{x}(s), s)\,\mathrm{d}s$ governs the tracer position. In this approach, a total of 7.55 M and 9.34 M particles were released inside the region of interest (aneurysmal region) of the AAA and CA models, respectively. The particles were released during ten equally spaced intracardiac time points. All particles were integrated until they left the region of interest. Subsequently, the spatiotemporal distribution of PRT was calculated, which was temporally averaged to obtain a single spatial distribution. The temporal averaging was done to enable comparison with the other methods.

2.2.2. Mean exposure time (MET)

In this approach, particles are densely seeded inside the region of interest and released during ten equally spaced intracardiac time points. After ten cardiac cycles of integration, the accumulated average time that all of the particles spend inside each computational element e is measured and normalized by element volume to obtain MET for each element (Lonyai et al., 2010; Shadden and Arzani, 2015)

$$\mathrm{MET}(e) = \frac{1}{N_e \sqrt[3]{V_e}} \sum_{p=1}^{N_t} \int_0^{\infty} H_e(p,t)\,\mathrm{d}t \tag{2}$$

$$H_e = \begin{cases} 1 & \text{if } \mathbf{x}_p(t) \in e \\ 0 & \text{if } \mathbf{x}_p(t) \notin e \end{cases},$$

where N_e is the number of times a particle passes through element e, V_e is the volume of the element, $\mathbf{x}_p(t)$ is the position of the tracer, H_e is the indicator function of the element e, and N_t is the total number of particles released. It should be pointed out that prior studies calculated MET by continuously releasing particles at the inlet (Lonyai et al., 2010; Arzani et al., 2014b). In the present study, particles were released uniformly in the region of interest to provide a reasonable correspondence with the Eulerian RT method. In both Lagrangian methods, an inward normal velocity of 0.005 cm/s was set at the no-slip wall to avoid particles sticking to the wall.

2.3. Eulerian methods

2.3.1. Eulerian RT (ERT)

ERT is computed by solving an advection-diffusion-reaction equation where the reaction term represents time, which is being integrated in an Eulerian framework. The equation is written as

$$\frac{\partial c}{\partial t} + \mathbf{u} \cdot \nabla c = \nabla \cdot (D \nabla c) + H \tag{3}$$
$$H = \begin{cases} 1 & \text{if } x \in \Gamma \\ 0 & \text{if } x \notin \Gamma \end{cases},$$

where c represents Eulerian RT (ERT), H is the source term, which is equal to 1 inside the region of interest and 0 outside this region, and D represents mass diffusivity set to 10^{-4} cm^2/s. The precise choice of D (as long as advection dominates) does not affect the results notably since the ERT solution does not involve near-wall boundary layers (Hansen et al., 2019). Zero Dirichlet boundary condition is imposed at the inlet and outlets. Zero flux boundary condition is applied at the wall. A higher value of D (0.05 cm^2/s) is applied near the outlet boundaries (outside the region of interest) to improve numerical convergence. The above equation was solved via the finite element method solver FEniCS (Logg et al., 2012) using linear tetrahedral elements. The equation was integrated for ten cardiac cycles until the solution reached steady state with intra-cardiac fluctuations. The final cardiac cycle was temporally averaged to define ERT.

2.3.2. Virtual-ink RT (RT_{VI})

In this method, RT is measured by virtually injecting a passive scalar at the inlet and monitoring the transport of the scalar throughout the flow domain by solving an advection-diffusion equation. The injected scalar represents a virtual ink. In the original approach (Rayz et al., 2010), virtual-ink RT was calculated by first establishing a fully ink-loaded model (by injecting ink at the inlet) and eventually injecting ink-free blood at the inlet and measuring the time that it takes for the inks to be washed away from the region of interest. Herein, an alternative approach is used. The initial condition (c_0) was set to 1 inside the region of interest (representing a uniform concentration of ink), zero concentration was prescribed at the inlet (representing ink-free blood), and zero flux boundary condition was applied at the wall. Subsequently, the advection-diffusion equation was solved.

$$\frac{\partial c}{\partial t} + \boldsymbol{u} \cdot \nabla c = \nabla \cdot (D \nabla c) \tag{4}$$
$$\mathrm{RT}_{VI} = \min(t) \in (0, \infty) \text{ s.t. } c = 0.02 c_0,$$

where D is selected same as above. It can take several cardiac cycles to achieve a complete flushing of the virtual inks. As a result, we ran the simulation for 15 cardiac cycles for AAA model and 4 cardiac cycles for CA model. After the aneurysms were completely flushed with ink-free blood, the RT was obtained through a post processing step where the time required for ink concentration to drop below a certain threshold (herein, 0.02) at a given point was measured.

2.3.3. Eulerian indicator RT (EIRT)

Recently, the concept of Eulerian indicators has been proposed to study transport and mixing using simple Eulerian measures (McIlhany and Wiggins, 2012). In this approach, the time required to travel a unit length from any given point in the direction of flow is measured with the consideration of mobility, which estimates net effective transport (McIlhany and Wiggins, 2012)

$$v_{fast}(\boldsymbol{x}) = \frac{1}{T}\left| \int_0^T \boldsymbol{v}(x,t) dt \right| \tag{5}$$
$$v_{slow}(\boldsymbol{x}) = \frac{1}{T} \int_0^T |\boldsymbol{v}(x,t)| dt$$
$$v_{sum}(\boldsymbol{x}) = (1 - e^{-\tilde{\omega}(\boldsymbol{x})}) v_{fast}(\boldsymbol{x}) + (e^{-\tilde{\omega}(\boldsymbol{x})}) v_{slow}(\boldsymbol{x}),$$

where $v_{fast}(\boldsymbol{x})$ is the magnitude of the time-average velocity vector, $v_{slow}(\boldsymbol{x})$ is the time-average of the velocity vector magnitude, $v_{sum}(\mathbf{x})$ represents mobility, and $\tilde{\omega}(\boldsymbol{x})$ is the relative rate of change of the velocity vector integrated in time:

$$\tilde{\omega}(\boldsymbol{x}) = \frac{1}{T} \int_0^T dw(\boldsymbol{x}, t) \tag{6}$$
$$dw(\boldsymbol{x}, t) = \frac{\|\boldsymbol{v}(\boldsymbol{x}, t + \Delta t) - \boldsymbol{v}(\boldsymbol{x}, t)\|}{\|\boldsymbol{v}(\boldsymbol{x}, t + \Delta t)\| + \|\boldsymbol{v}(\boldsymbol{x}, t)\|}.$$

The inverse of mobility represents an estimate of flow stagnation, herein denoted as Eulerian Indicator RT (EIRT):

$$\mathrm{EIRT} = \frac{1}{v_{sum}}. \tag{7}$$

The integration time (T) in the above equations was set to the corresponding cardiac cycle duration.

2.3.4. Point-wise RT (RT_{PW})

Point-wise RT is defined as the inverse of time-average velocity at each point (Esmaily-Moghadam et al., 2013):

$$\mathrm{RT}_{PW} = \left(\frac{1}{T} \int_0^T \|\boldsymbol{u}(\boldsymbol{x}, t)\| dt \right)^{-1}. \tag{8}$$

RT_{PW} and EIRT measures are not defined on the vessel wall as the velocity is zero due to no-slip condition.

3. Results

Figs. 2 and 3 show the surface RT patterns of AAA and CA models, respectively. RT_{PW} and EIRT are not defined on the wall and therefore not shown. Lagrangian coherent structures (LCS) in the WSS vector field (WSS LCS) (Arzani et al., 2016, 2017) are computed from stable and unstable manifolds of time-average WSS vector field (explained in (Arzani et al., 2017)) and shown on the left panel for comparison. RT results obtained from the two Eulerian methods (ERT and RT_{VI}) show somewhat similar near-wall patterns. A similar observation is made for the Lagrangian PRT and MET methods, yet their distinctions are more pronounced. The Eulerian and Lagrangian class of methods demonstrate mostly different near-wall RT patterns. In the Eulerian methods, elevated near-wall RT occurs in the proximity of the attracting WSS LCS. On the other hand, elevated Lagrangian RT values are close to the repelling WSS LCS.

RT patterns inside AAA and CA models can be visualized from Figs. 4–7. Two different cross-sections are shown in these figures. EIRT and Point-wise RT results are identical. The PRT field demonstrates patterns mostly different than other approaches. An overall similar qualitative pattern with some distinctive features can be seen for the other methods.

Quantitatively, all of the techniques manifest different maximum RT values. The maximum values of RT and 99 percentile of maximum RT values obtained using different approaches are tabulated in Table 1. As expected, different values are obtained from each method. Spearman's rank correlation coefficients between all methods are shown for the AAA and CA models in Tables 2 and 3, respectively. The correlation coefficients show that ERT has a high correlation with RT_{VI}. MET has a high correlation with EIRT and RT_{PW}. The correlations of PRT with all of the other approaches are lower. EIRT and RT_{PW} are highly correlated.

4. Discussion

This study explored different RT definitions utilized for measuring flow stagnation in cardiovascular flows. The RT measures are classified into Lagrangian and Eulerian methods. The Lagrangian methods calculate flow stagnation via discrete particle tracking, whereas the Eulerian methods measure flow stagnation based on

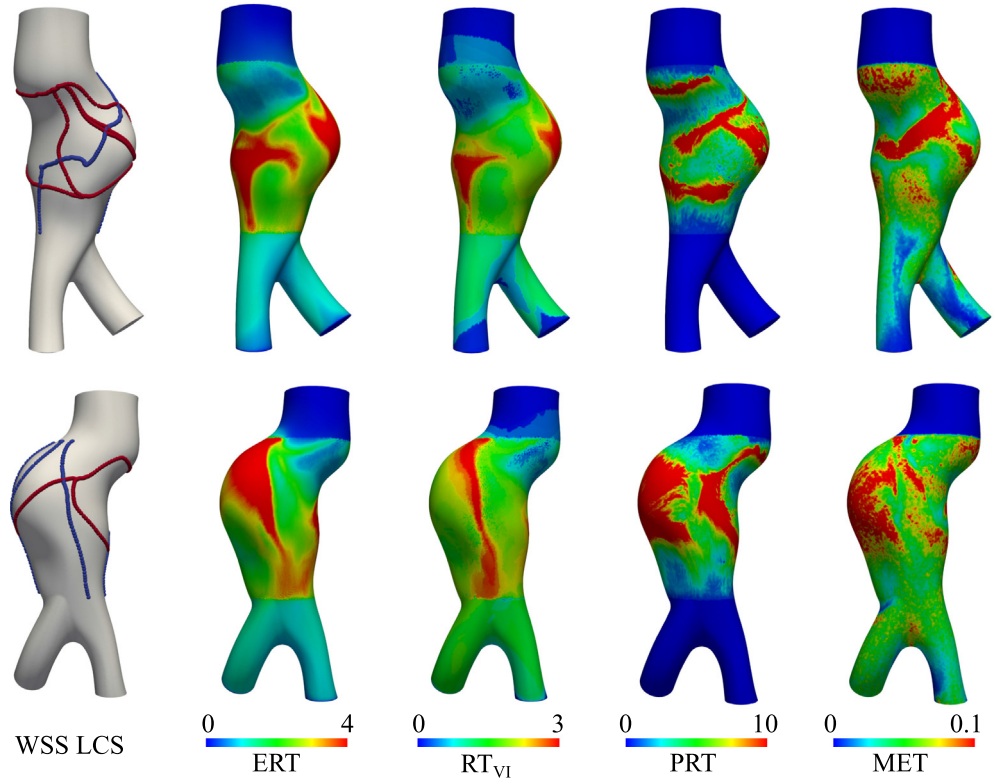

Fig. 2. Front and back view of different surface residence time (RT) measures are shown in the AAA model. WSS LCS (attracting-blue, repelling-red) are shown on the left panel. Eulerian RT (ERT), virtual-ink RT (RT_{VI}), particle residence time (PRT), and mean exposure time (MET) approaches are shown. The unit of ERT, RT_{VI}, and PRT is seconds whereas the unit of MET is s/cm.

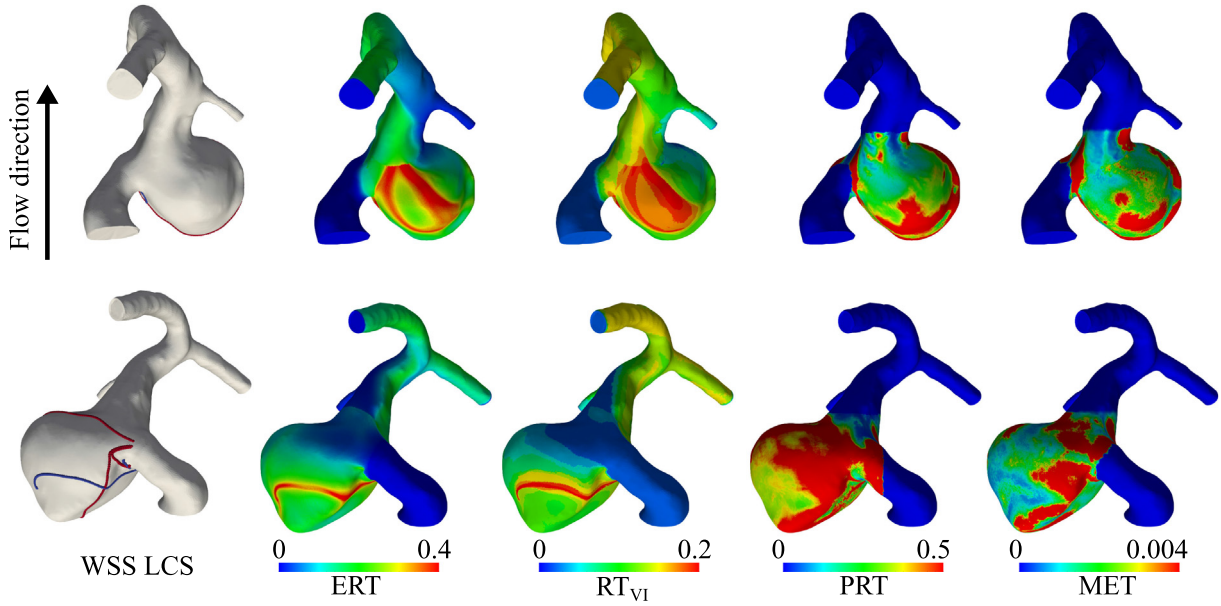

Fig. 3. Front and back view of different surface residence time (RT) measures are shown in the CA model. WSS LCS (attracting-blue, repelling-red) are shown on the left panel. Eulerian RT (ERT), virtual-ink RT (RT_{VI}), particle residence time (PRT), and mean exposure time (MET) approaches are shown. The unit of ERT, RT_{VI}, and PRT is seconds whereas the unit of MET is s/cm. (For interpretation of the references to color in this figure legend, the reader is referred to the web version of this article.)

continuum partial differential equations or simple measures based on velocity. Herein, all of these methods were qualitatively and quantitatively compared in a patient-specific AAA and a CA model. Different flow solvers, boundary conditions, and spatiotemporal resolutions were used for each aneurysm, however, for each model, the same velocity field was used for all RT calculations.

Our results emphasize the distinction between the above methods. Generally, each method not only calculates flow stagnation in a different fashion but also conceptually has a different definition of RT and flow stagnation. This results in pronounced distinctions between some of the methods. In particular, PRT shows the least correlation with all of the other methods. PRT depends upon the

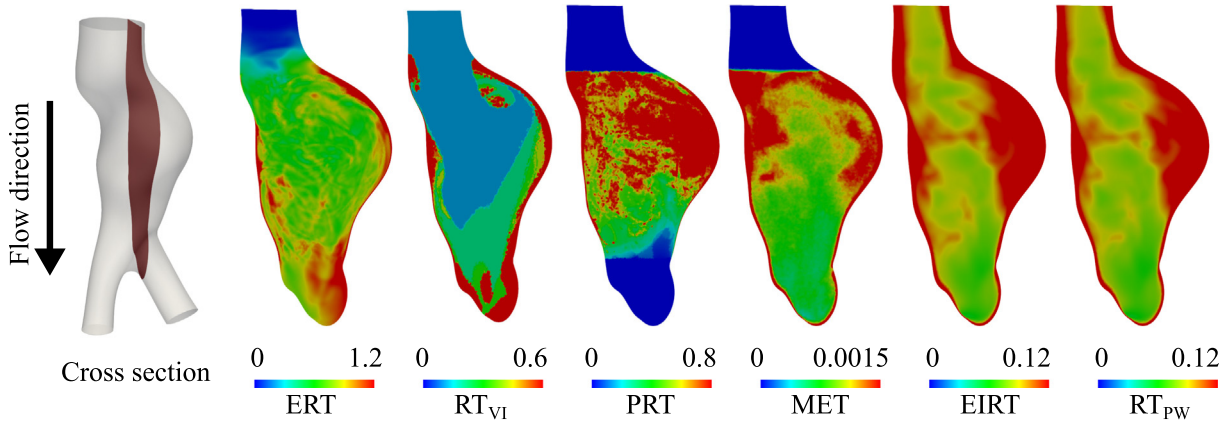

Fig. 4. Cross section of residence time (RT) in the AAA model. Eulerian RT (ERT), virtual-ink RT (RT_{VI}), particle residence time (PRT), mean exposure time (MET), Eulerian indicator RT (EIRT), and point-wise RT (RT_{PW}) approaches are shown. The unit of ERT, RT_{VI}, and PRT is seconds whereas the unit of MET, EIRT, and RT_{PW} is s/cm.

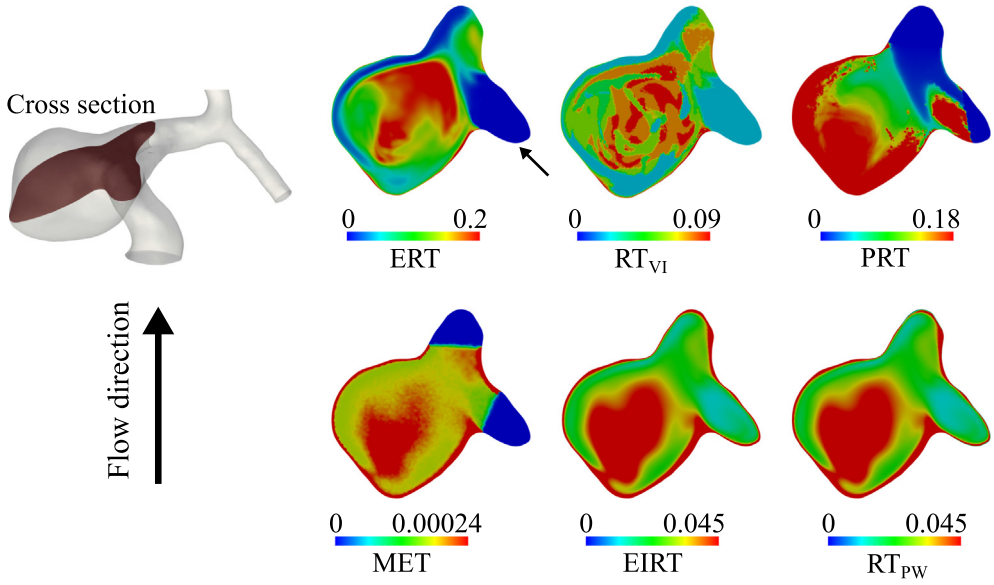

Fig. 5. Cross section of residence time (RT) in the CA model. Eulerian RT (ERT), virtual-ink RT (RT_{VI}), particle residence time (PRT), mean exposure time (MET), Eulerian indicator RT (EIRT), and point-wise RT (RT_{PW}) approaches are shown. The unit of ERT, RT_{VI}, and PRT is seconds whereas the unit of MET, EIRT, and RT_{PW} is s/cm.

characteristic length of the region of interest, which makes it distinct from the other definitions of RT. Additionally, PRT is defined based on individual particle behavior and does not represent flow stagnation locally. That is, a particle released at a certain location may spend a long time inside the aneurysm, however, not necessarily at the same location where it was released. Since PRT maps back the RT value to the initial location of particle release, it cannot describe the actual location that the particle resides. MET has been proposed to mitigate the shortcomings of PRT. MET maintains a stronger correlation with the Eulerian approaches and is moderately correlated to PRT. However, MET requires a high resolution of Lagrangian tracers to be seeded and released in order to sample all of the computational elements adequately. Therefore, it is advisable to use an auxiliary mesh with elements larger than the flow solver elements in MET calculation. It is noteworthy that quantitative MET values are by definition sensitive to element size. However, we confirmed that making the MET mesh edge size 40% larger minimally affects the qualitative results and correlation coefficients. Accurate 3D particle tracking near the vessel wall is another complication of Lagrangian methods (Arzani et al., 2016). Another difficulty associated with Lagrangian methods is handling diffusion. While random walk models can be implemented to model diffusion (Ghosh et al., 1998), these methods typically require a large number of releases for statistical sampling. The Eulerian continuum methods handle diffusion inherently via the diffusion term.

The Lagrangian methods offer some advantages. First, these methods are calculated from post-processing discrete tracers. Therefore, a clear correspondence with transport is made where transport of individual tracers can be visualized and their effect on RT studied. This leads to a nice correspondence with flow topology where a close connection between PRT, LCS, and finite-time Lyapunov exponents can be established (Shadden and Taylor, 2008). Additionally, PRT computation is very efficient as tracers are independent of each other. If one is only interested in a small subset of the domain then a few tracers can be released at that location to calculate PRT locally. Finally, inertial particles can easily be modeled using discrete particle tracking (Shadden and Arzani, 2015) and PRT/MET measures can be readily adapted for them.

Regarding Eulerian methods, ERT demonstrates RT patterns similar to RT_{VI} and a relatively high correlation exists between these methods. Both methods are based on continuum transport

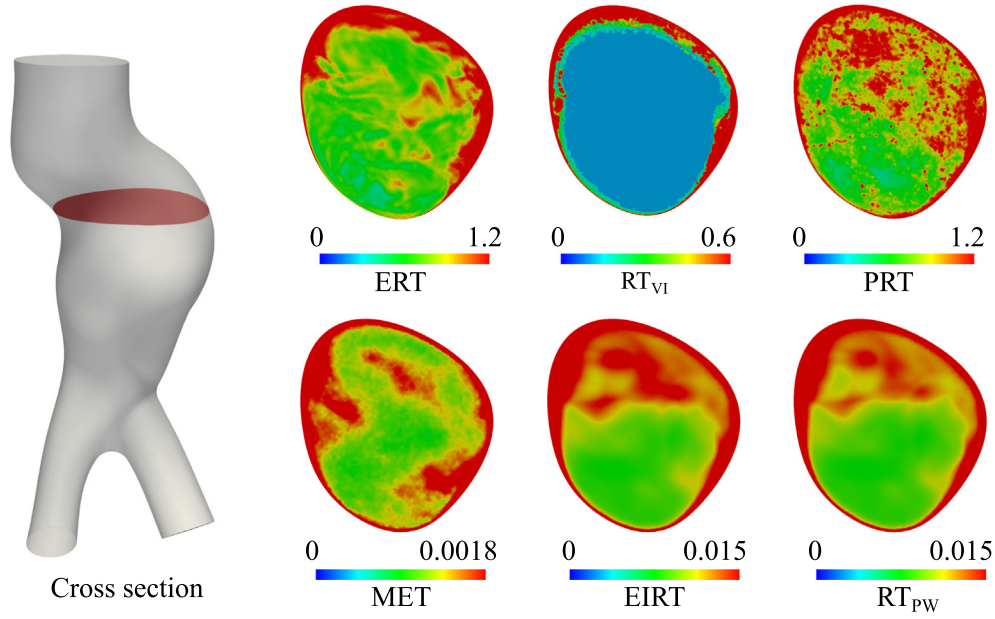

Fig. 6. Cross section of residence time (RT) in the AAA model. Eulerian RT (ERT), virtual-ink RT (RT_{VI}), particle residence time (PRT), mean exposure time (MET), Eulerian indicator RT (EIRT), and point-wise RT (RT_{PW}) approaches are shown. The unit of ERT, RT_{VI}, and PRT is seconds whereas the unit of MET, EIRT, and RT_{PW} is s/cm.

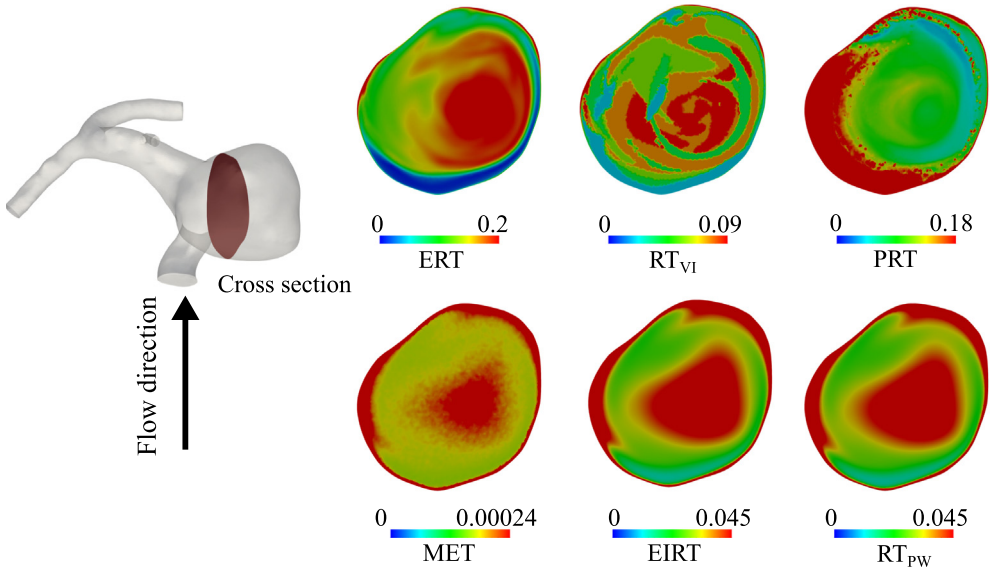

Fig. 7. Cross section of residence time (RT) in the CA model. Eulerian RT (ERT), virtual-ink RT (RT_{VI}), particle residence time (PRT), mean exposure time (MET), Eulerian indicator RT (EIRT), and point-wise RT (RT_{PW}) approaches are shown. The unit of ERT, RT_{VI}, and PRT is seconds whereas the unit of MET, EIRT, and RT_{PW} is s/cm.

Table 1
Maximum RT values obtained from six different approaches.

Approach	Maximum RT (AAA)	Maximum RT (CA)	99 percentile RT (AAA)	99 percentile RT (CA)
$ERT(s)$	7.88	0.655	4.63	0.34
$RT_{VI}(s)$	13.37	1.05	8.63	0.66
$PRT(s)$	15.32	6.25	13.07	1.62
$MET(s/cm)$	0.02	0.13	0.01	0.01
$EIRT(s/cm)$	16.93	10.60	7.24	0.91
$RT_{PW}(s/cm)$	13.58	5.56	6.49	0.88

models similar to convective heat transfer, therefore we can make an analogy of these methodologies with heat transfer problems where time is replaced with temperature. In the ERT approach, the region of interest is continuously and uniformly heated and a cold stream of fluid is allowed to enter into this region through the inlet. The cold fluid mixes with the hot fluid as the incoming flow enters the region of interest. After sufficient integration, the temperature reaches a steady state with intra-cardiac fluctuations.

Table 2
Spearman's rank correlation coefficient among the investigated approaches for the AAA model. All correlation coefficients were statistically significant.

Approach	RT_{VI}	PRT	MET	EIRT	RT_{PW}
ERT	0.82	0.25	0.48	0.62	0.61
RT_{VI}		0.34	0.61	0.74	0.74
PRT			0.68	0.60	0.60
MET				0.87	0.87
EIRT					0.99

Table 3
Spearman's rank correlation coefficient among the investigated approaches for the CA model. All correlation coefficients were statistically significant.

Approach	RT_{VI}	PRT	MET	EIRT	RT_{PW}
ERT	0.81	−0.18	0.23	0.35	0.35
RT_{VI}		−0.15	0.15	0.25	0.25
PRT			0.44	0.29	0.29
MET				0.93	0.93
EIRT					0.99

The incoming cold fluid leaves its trace as it passes through the region of interest. This can clearly be seen in Fig. 5 where a low RT region is created next to the wall (blue region) as the incoming flow shears the aneurysm wall. In the RT_{VI} approach, initially, the region of interest is filled with uniformly hot fluid, which is later allowed to exit the region of interest and also mix with the cold flow coming from the inlet. Subsequently, the time it takes for each element to cool down is measured. In the original study, Rayz et al. (2010) interpreted the hot fluid as virtual ink and the cold fluid as an ink-free domain. Another useful interpretation of RT_{VI} is correspondence with virtual contrast agents where the transit time of virtual contrast agents can be studied to guide contrast-enhanced imaging modalities.

Finally, RT_{PW} and EIRT are simple measures that estimate RT based on the local velocity field. Therefore, these methods fail to capture the emergent transport behavior and mixing that depend on the global flow characteristics. However, these measures had a reasonable correlation with the other methods, implying that they may be used as an approximate yet efficient method to estimate flow stagnation. EIRT improves the RT_{PW} definition by considering both fast and slow changing flows. However, for the models studied here, both definitions produced qualitatively identical results. We anticipate the EIRT measure to stand out when significant temporal oscillation in velocity vector direction exists. It is noteworthy that RT_{PW} is similar to relative residence time (RRT), a measure of near-wall stagnation based on WSS, while EIRT is similar to the oscillatory shear index (Arzani et al., 2017). Note that RT_{PW} defines RT based on inverse of time-average velocity magnitude as opposed to inverse of magnitude of time-average WSS vector in RRT.

Our study emphasizes that each approach depicts distinct quantitative RT values (Table 1), which was expected given the distinct definitions of RT in each method (even in the methods with similar RT units). It should be mentioned that even though MET has units similar to EIRT and RT_{PW}, its definition is very different. MET measures accumulated amount of time spent by all particles inside each element normalized by element length scale, while EIRT and RT_{PW} measure inverse velocity. Among the other three methods that measure time, PRT quantifies the highest values. This is anticipated as discrete Lagrangian methods are influenced by individual particle behavior while Eulerian methods quantify a smoothed continuum behavior (Hansen et al., 2015).

An interesting observation was the close connection between near-wall RT and WSS LCS. The concept of WSS LCS was recently proposed to study near-wall transport and biochemical surface concentration patterns (Arzani et al., 2016, 2017; Farghadan and Arzani, 2019). Herein, we have shown that these structures also influence RT patterns close to the wall. Regions of high near-wall RT in the Eulerian continuum methods (ERT and RT_{VI}) match the attracting WSS LCS (Figs. 2 and 3). This implies that the Eulerian continuum methods' definition of RT is tightly related to concentration. In other words, high stagnation can also imply high concentration in the context of mass transport. On the other hand, EIRT and RT_{PW} provide a pure definition of stagnation. Namely, if the velocity at a location is predominantly low then high flow stagnation exists there. In the context of near-wall transport, a similar conclusion was previously made for WSS exposure time (WSSET) and RRT. Namely, WSSET can measure near-wall stagnation and concentration, whereas RRT only measures near-wall stagnation (Arzani et al., 2017). These results should not be surprising since the governing equations in the continuum RT methods can correspond to a mass transport problem (similar to the above heat transfer analogy). Loosely speaking, this implies that we may think of RT in these methods as "concentration of time". Another interesting observation was that regions of high near-wall PRT typically coincide with the repelling WSS LCS (Figs. 2 and 3). This can be explained as follows. The near-wall normal velocity in the vicinity of repelling WSS LCS is towards the wall. Therefore, tracers that are released next to the repelling WSS LCS travel near the wall for a long time and are eventually attracted towards an attracting WSS LCS where they accumulate. Therefore, by definition, these locations have high PRT values.

An important question remains to be answered: which RT method should we use? We believe that there is not a single answer to this question. Most of the methods are conceptually different and should not be considered the same. ERT is suitable if one is interested in RT in the context of biochemical mass transport and concentration. RT_{VI} is appropriate if one is interested in the time that it takes for an initially uniformly distributed concentration of biochemicals to drop below a certain threshold. PRT is suitable if one is interested in individual particle behavior and wants to quantify RT related to the location of release. Regarding MET, it is suggested that ERT be used instead unless one wants to take advantage of the flexibilities associated with Lagrangian particle tracking. Finally, RT_{PW} and EIRT are suitable if one wants to quickly estimate RT without any transport model.

This work highlights the distinctions in different methods used in the literature to measure flow stagnation and suggests that the RT method should be selected based on the method's conceptual definition of flow stagnation and the application of interest.

Conflict of interest

None.

Acknowledgement

Support from Northern Arizona University's high-performance computing cluster Monsoon is acknowledged.

References

Arzani, A., Gambaruto, A.M., Chen, G., Shadden, S.C., 2016. Lagrangian wall shear stress structures and near-wall transport in high-schmidt-number aneurysmal flows. J. Fluid Mech. 790, 158–172.
Arzani, A., Gambaruto, A.M., Chen, G., Shadden, S.C., 2017. Wall shear stress exposure time: a lagrangian measure of near-wall stagnation and concentration in cardiovascular flows. Biomech. Model. Mechanobiol. 16 (3), 787–803.
Arzani, A., Les, A.S., Dalman, R.L., Shadden, S.C., 2014a. Effect of exercise on patient specific abdominal aortic aneurysm flow topology and mixing. Int. J. Numer. Methods Biomed. Eng. 30 (2), 280–295.

Arzani, A., Shadden, S.C., 2012. Characterization of the transport topology in patient-specific abdominal aortic aneurysm models. Phys. Fluids 24 (8), 081901.
Arzani, A., Suh, G.Y., Dalman, R.L., Shadden, S.C., 2014b. A longitudinal comparison of hemodynamics and intraluminal thrombus deposition in abdominal aortic aneurysms. Am. J. Physiol. Heart Circulatory Physiol. 307 (12), H1786–H1795.
Assar, A.N., Zarins, C.K., 2009. Ruptured abdominal aortic aneurysm: a surgical emergency with many clinical presentations. Postgrad. Med. J. 85 (1003), 268–273.
Boussel, L., Rayz, V., McCulloch, C., Martin, A., Acevedo-Bolton, G., Lawton, M., Higashida, R., Smith, W.S., Young, W.L., Saloner, D., 2008. Aneurysm growth occurs at region of low wall shear stress: patient-specific correlation of hemodynamics and growth in a longitudinal study. Stroke 39 (11), 2997–3002.
Brisman, J.L., Song, J.K., Newell, D.W., 2006. Cerebral aneurysms. N. Engl. J. Med. 355 (9), 928–939.
Butty, V.D., Gudjonsson, K., Buchel, P., Makhijani, V.B., Ventikos, Y., Poulikakos, D., 2002. Residence times and basins of attraction for a realistic right internal carotid artery with two aneurysms. Biorheology 39 (3, 4), 387–393.
Chiu, J.J., Chen, C.N., Lee, P.L., Yang, C.T., Chuang, H.S., Chien, S., Usami, S., 2003. Analysis of the effect of disturbed flow on monocytic adhesion to endothelial cells. J. Biomech. 36 (12), 1883–1895.
Dickson, B.C., 2004. Venous thrombosis: on the history of virchow's triad. Univ. Toronto Med. J. 81 (3), 166–171.
Duvernois, V., Marsden, A.L., Shadden, S.C., 2013. Lagrangian analysis of hemodynamics data from FSI simulation. Int. J. Numer. Methods Biomed. Eng. 29 (4), 445–461.
Epshtein, M., Korin, N., 2018. Mapping the transport kinetics of molecules and particles in idealized intracranial side aneurysms. Sci. Rep. 8 (1), 8528.
Esmaily-Moghadam, M., Hsia, T., Marsden, A.L., 2013. A non-discrete method for computation of residence time in fluid mechanics simulations. Phys. Fluids 25 (11), 110802.
Farghadan, A., Arzani, A., 2019. The combined effect of wall shear stress topology and magnitude on cardiovascular mass transport. Int. J. Heat Mass Transf. 131, 252–260.
Ghosh, S., Leonard, A., Wiggins, S., 1998. Diffusion of a passive scalar from a no-slip boundary into a two-dimensional chaotic advection field. J. Fluid Mech. 372, 119–163.
Hansen, K.B., Arzani, A., Shadden, S.C., 2015. Mechanical platelet activation potential in abdominal aortic aneurysms. J. Biomech. Eng. 137 (4), 041005.
Hansen, K.B., Arzani, A., Shadden, S.C., 2019. Finite element modeling of near-wall mass transport in cardiovascular flows. Int. J. Numer. Methods Biomed. Eng. 35 (1), e3148.
Hoi, Y., Wasserman, B.A., Xie, Y.J., Najjar, S.S., Ferruci, L., Lakatta, E.G., Gerstenblith, G., Steinman, D.A., 2010. Characterization of volumetric flow rate waveforms at the carotid bifurcations of older adults. Physiol. Meas. 31 (3), 291.
Humphrey, J.D., Taylor, C.A., 2008. Intracranial and abdominal aortic aneurysms: similarities, differences, and need for a new class of computational models. Annu. Rev. Biomed. Eng. 10, 221–246.
Ku, D.N., Giddens, D.P., Zarins, C.K., Glagov, S., 1985. Pulsatile flow and atherosclerosis in the human carotid bifurcation. Positive correlation between plaque location and low oscillating shear stress. Arterioscl. Off. J. Am. Heart Assoc. Inc. 5 (3), 293–302.
Kunov, M.J., Steinman, D.A., Ethier, C.R., 1996. Particle volumetric residence time calculations in arterial geometries. J. Biomech. Eng. 118 (2), 158–164.
Les, A.S., Shadden, S.C., Figueroa, C.A., Park, J.M., Tedesco, M.M., Herfkens, R.J., Dalman, R.L., Taylor, C.A., 2010. Quantification of hemodynamics in abdominal aortic aneurysms during rest and exercise using magnetic resonance imaging and computational fluid dynamics. Ann. Biomed. Eng. 38 (4), 1288–1313.
Logg, A., Mardal, K.A., Wells, G., 2012. Automated solution of differential equations by the finite element method, vol. 84. Springer, Berlin, Heidelberg.
Long, C.C., Esmaily-Moghadam, M., Marsden, A.L., Bazilevs, Y., 2014. Computation of residence time in the simulation of pulsatile ventricular assist devices. Comput. Mech. 54 (4), 911–919.
Lonyai, A., Dubin, A.M., Feinstein, J.A., Taylor, C.A., Shadden, S.C., 2010. New insights into pacemaker lead-induced venous occlusion: simulation-based investigation of alterations in venous biomechanics. Cardiovasc. Eng. 10 (2), 84–90.
Lowe, G.D.O., 2003. Virchow's triad revisited: abnormal flow. Pathophysiol. Haemost. Thromb. 33 (5–6), 455–457.
Martufi, G., Gasser, T.C., 2013. The role of biomechanical modeling in the rupture risk assessment for abdominal aortic aneurysms. J. Biomech. Eng. 135 (2), 021010.
McIlhany, K.L., Wiggins, S., 2012. Eulerian indicators under continuously varying conditions. Phys. Fluids 24 (7), 073601.
Meng, H., Tutino, V.M., Xiang, J., Siddiqui, A., 2013. High WSS or low WSS? Complex interactions of hemodynamics with intracranial aneurysm initiation, growth, and rupture: toward a unifying hypothesis. Am. J. Neuroradiol.
Mortensen, M., Valen-Sendstad, K., 2015. Oasis: A high-level/high-performance open source Navier–Stokes solver. Comput. Phys. Commun. 188, 177–188.
Narracott, A., Smith, S., Lawford, P., Liu, H., Himeno, R., Wilkinson, I., Griffiths, P., Hose, R., 2005. Development and validation of models for the investigation of blood clotting in idealized stenoses and cerebral aneurysms. J. Artif. Organs 8 (1), 56–62.
Nerem, R.M., 1992. Vascular fluid mechanics, the arterial wall, and atherosclerosis. J. Biomech. Eng. 114 (3), 274–282.
Perktold, K., 1987. On the paths of fluid particles in an axisymmetrical aneurysm. J. Biomech. 20 (3), 311–317.
Raffort, J., Lareyre, F., Clément, M., Hassen-Khodja, R., Chinetti, G., Mallat, Z., 2017. Monocytes and macrophages in abdominal aortic aneurysm. Nat. Rev. Cardiol. 14 (8), 457.
Rayz, V.L., Boussel, L., Ge, L., Leach, J.R., Martin, A.J., Lawton, M.T., McCulloch, C., Saloner, D., 2010. Flow residence time and regions of intraluminal thrombus deposition in intracranial aneurysms. Ann. Biomed. Eng. 38 (10), 3058–3069.
Rossini, L., Martinez-Legazpi, P., Vu, V., Fernández-Friera, L., del Villar, C.P., Rodríguez-López, S., Benito, Y., Borja, M., Pastor-Escuredo, D., Yotti, R., et al., 2016. A clinical method for mapping and quantifying blood stasis in the left ventricle. J. Biomech. 49 (11), 2152–2161.
Satta, J., Läärä, E., Juvonen, T., 1996. Intraluminal thrombus predicts rupture of an abdominal aortic aneurysm. J. Vasc. Surg. 23 (4), 737–739.
Sengupta, D., Kahn, A.M., Burns, J.C., Sankaran, S., Shadden, S.C., Marsden, A.L., 2012. Image-based modeling of hemodynamics in coronary artery aneurysms caused by Kawasaki disease. Biomech. Model. Mechanobiol. 11 (6), 915–932.
Shadden, S.C., Arzani, A., 2015. Lagrangian postprocessing of computational hemodynamics. Ann. Biomed. Eng. 43 (1), 41–58.
Shadden, S.C., Taylor, C.A., 2008. Characterization of coherent structures in the cardiovascular system. Ann. Biomed. Eng. 36 (7), 1152–1162.
Suh, G.Y., Les, A.S., Tenforde, A.S., Shadden, S.C., Spilker, R.L., Yeung, J.J., Cheng, C.P., Herfkens, R.J., Dalman, R.L., Taylor, C.A., 2011a. Hemodynamic changes quantified in abdominal aortic aneurysms with increasing exercise intensity using MR exercise imaging and image-based computational fluid dynamics. Ann. Biomed. Eng. 39 (8), 2186–2202.
Suh, G.Y., Les, A.S., Tenforde, A.S., Shadden, S.C., Spilker, R.L., Yeung, J.J., Cheng, C.P., Herfkens, R.J., Dalman, R.L., Taylor, C.A., 2011b. Quantification of particle residence time in abdominal aortic aneurysms using magnetic resonance imaging and computational fluid dynamics. Ann. Biomed. Eng. 39 (2), 864–883.
Tambasco, M., Steinman, D.A., 2002. On assessing the quality of particle tracking through computational fluid dynamic models. J. Biomech. Eng. 124 (2), 166–175.
Updegrove, A., Wilson, N.M., Merkow, J., Lan, H., Marsden, A.L., Shadden, S.C., 2017. Simvascular: an open source pipeline for cardiovascular simulation. Ann. Biomed. Eng. 45 (3), 525–541.
Valen-Sendstad, K., Piccinelli, M., KrishnankuttyRema, R., Steinman, D.A., 2015. Estimation of inlet flow rates for image-based aneurysm CFD models: where and how to begin? Ann. Biomed. Eng. 43 (6), 1422–1431.
Wolf, Y.G., Thomas, W.S., Brennan, F.J., Goff, W.G., Sise, M.J., Bernstein, E.F., 1994. Computed tomography scanning findings associated with rapid expansion of abdominal aortic aneurysms. J. Vasc. Surg. 20 (4), 529–538.